Mon. Not. R. Astron. Soc. **000**, 1–9 (2008) Printed 8 April 2008 (MN LATEX style file v2.2)

Young Globular Clusters in an old S0: Clues to the Formation History of NGC 4570⋆

R. Kotulla[1]†, U. Fritze[1] and P. Anders[2]
[1] *Centre for Astrophysics Research, University of Hertfordshire, College Lane, Hatfield AL10 9AB, United Kingdom*
[2] *Sterrenkundig Instituut, Universiteit Utrecht, P.O. Box 80000, NL-3508 TA Utrecht, The Netherlands*

Accepted April 05, 2008. Received March 26, 2008; in original form February 04, 2008

ABSTRACT

We here present our first attempt to use Globular Clusters as tracers of their parent galaxy's formation history. Globular Cluster Systems of most early-type galaxies feature two peaks in their optical colour distributions. Blue-peak Globular Clusters are generally believed to be old and metal-poor. The ages, metallicities, and the origin of the red-peak Globular Clusters are being debated. We here present our analysis of the ages and metallicities of the red peak Globular Clusters in the Virgo S0 NGC 4570 using deep K_s-band photometry from NTT/SOFI (ESO program ID 079.B-0511) for the red-peak Globular Clusters in combination with HST-ACS archival data to break the age-metallicity degeneracy.

We analyze the combined g, z, and K_s spectral energy distribution by comparison with a large grid of GALEV evolutionary synthesis models for star clusters with different ages and metallicities. This analysis reveals a substantial population of intermediate-age (1–3 Gyr) and metal-rich (≈ solar metallicity) Globular Clusters. We discuss their age and metallicity distributions together with information on the parent galaxy from the literature to gain insight into the formation history of this galaxy.

Our results prove the power of this approach to reveal the (violent) star formation and chemical enrichment histories of galaxies on the basis of combined optical and near-infrared photometry.

Key words: galaxies: individual: NGC 4570 – galaxies: star clusters – galaxies: lenticular – galaxies: formation.

1 INTRODUCTION

Globular Cluster (GC) systems are now recognized as powerful tracers of their parent galaxy's formation history (West et al. 2004; Fritze-v. Alvensleben 2004; Brodie & Strader 2006). From their age and metallicity distributions one can reconstruct the parent galaxy's (violent) star formation and chemical enrichment histories all the way from the very onset of star formation in the Early Universe to the present.

Most early-type galaxies show bimodal color distributions for their GC systems (e.g. Gebhardt & Kissler-Patig 1999; Kundu & Whitmore 2001a,b; Peng et al. 2006): A universal blue peak and a red peak for which the color and height relative to the blue peak vary from galaxy to galaxy. The blue peak GCs are generally agreed to be old and metal-poor, the properties and origin of the red peak GCs is still unclear. Scenarios for the formation of the red peak GCs range from *in situ* formation of a secondary more metal-rich population of GCs within their parent galaxy shortly after the first one (Forbes et al. 1997) to major gas-rich mergers (e.g. Ashman & Zepf 1992) and hierarchical accretion events involving enough gas to trigger the formation of new GC populations (e.g. Beasley et al. 2002). The age distributions of the secondary GCs predicted by these different scenarios are different: almost as old as the old and metal-poor blue peak GCs but more metal-rich than those in the first case, of some intermediate age reflecting the time of the gas-rich merger in the second case, and broad or multi-peaked for a series of hierarchical accretion events involving gas in the third case. The metallicities of the secondary, and eventually any further generations of GCs should reflect the ISM abundances in the merging or accreted objects at the time of merging or accretion. They could, at most, be somewhat higher for those GCs that formed late enough in a burst to already incorporate some enrichment during the burst itself.

⋆ Based on observations made with ESO Telescopes at the La Silla Observatory under programme ID 079.B-0511
† E-mail: r.kotulla@herts.ac.uk

Hierarchical accretion without gas and the formation of new generations of GCs cannot explain the red-peak GCs since dwarf galaxies known so far contain old and metal-poor, hence blue GCs.

To determine the ages and metallicities of the red-peak GCs in one of those early-type galaxies with clear bimodality in its optical GC colour distribution is the aim of our present investigation and should help constrain the formation scenario for the red-peak GCs in this particular galaxy.

1.1 Our approach to lift the age-metallicity degeneracy

Optical data alone do **not** allow to disentangle ages and metallicities: Colour-to-metallicity transformations have to assume an age, while colour-to-age transformations are only valid for one metallicity. The degeneracy, however, can be broken by including near-infrared data that are more sensitive to metallicity rather than to age.

Anders et al. (2004) used extensive artificial star cluster tests and showed that observations in three passbands for GCs in dust-free E/S0s (or four passbands for young star clusters in dusty environments), spanning as wide as possible a wavelength-basis (U through K) and including at least one NIR-band (e.g. H or K) with photometric accuracies $\leqslant 0.05$ mag in the optical and $\leqslant 0.1$ mag in the NIR allow to disentangle ages and metallicities and to determine **individual GC metallicities to** $< \pm 0.2$ **dex, and ages to** $< \pm 0.3$ **dex**. I.e., these data allow to distinguish $\leqslant 7$ Gyr old GCs from those $\geqslant 13$ Gyr old.

Similar studies also using NIR-data to determine ages and metallicities of globular clusters have only been done for a few galaxies until now (Puzia et al. 2002; Kissler-Patig et al. 2002; Hempel et al. 2003; Larsen et al. 2005; Hempel et al. 2007). More than half of these galaxies were found to host a population of GCs that is younger and/or more metal-rich than the ubiquitous old and metal-poor GC population.

Some of these previous studies discussed average properties of the blue and red peak GCs by investigating the mean colours of blue and red GC. We here derive ages, metallicities, and masses for every individual cluster with (g, z, K) photometry. This also enables us to study whether there is more than one generation of GCs in the red peak, to look for correlations of these parameters, and investigate their spatial distributions.

We have chosen the Virgo cluster S0 galaxy NGC4570 (= VCC1692) for our pilot study because it has archival $g-$ and $z-$band data from the ACS Virgo Cluster Project (Peng et al. 2006) that show two very clear peaks in the optical $g-z$ colour distribution of its GC system. The red peak is about two thirds the height of the blue one, both have very similar widths. In particular, the optical colour distribution shows no evidence for substructure within the red peak or for a third peak. The mean $g-z$ colours of the blue and red peaks are 0.88 ± 0.01 and 1.38 ± 0.03, respectively, with a fraction of 39 % of all the 122 GCs detected belonging to the red peak. NGC4570 has $B_T = 11.82$ mag (Côté et al. 2006), which at a kinematic distance modulus of $BDM = 31.16$ (Mei et al. 2007) gives it an absolute $M_B = -19.3$ mag, i.e. it is an average luminosity S0.

van den Bosch et al. (1998) and van den Bosch & Emsellem (1998) detected a nuclear stellar disk with a radial extent of ≈ 7 arcsec. From both spectroscopy based on Hβ and [MgFe] line indices as well as photometry in U, V and I they estimate an age of the stellar population inside that structure of $\leqslant 2$ Gyr and a metallicity close to solar.

From the same ACS Virgo Cluster survey that reported the GC colours Ferrarese et al. (2006) show that NGC 4570 shows a nested-disk structure composed of two morphologically distinct inner and out disks. Detailed isophotal analysis reveals a blue stellar ring with radius 150 pc, but less than 7 pc wide, around the nucleus. This ring leaves a clear imprint on the major axis $g-$band surface brightness profile (cf. Fig. 104 of Ferrarese et al. 2006). The structure of this inner region was discussed by van den Bosch & Emsellem (1998) in the context of secular bar evolution.

2 MODELS

We used our GALEV evolutionary synthesis models for star clusters (Schulz et al. 2002; Anders & Fritze-v. Alvensleben 2003) to compute a large grid of models for five different metallicities $-1.7 \leqslant$ [Fe/H] $\leqslant +0.4$ and ages between 4 Myr and 16 Gyr in time-steps of 4 Myr. Our models are based on Padova isochrones and a Salpeter (1955) initial mass function (IMF) with a lower-mass limit of $M_{low} = 0.10$ $M_\odot$ and upper mass limits between $M_{up} \approx 50 - 70$ $M_\odot$ depending on metallicity.

Since early-type galaxies in general, and NGC 4570 in particular, do not contain significant amounts of dust we did not include internal extinction into our grid but assume E(B − V) = 0 throughout. We therefore only need three filters (HST F475W, F850LP and SOFI K_s) to determine all relevant parameters (age, metallicity, and mass) for each cluster.

Note that we do not depend on color transformations from the HST to Standard Johnson filters. For optimal accuracies, our models first compute spectra as a function of time, that later are convolved with the corresponding filter curves, in this case for the HST F475W and F850LP filters and the SOFI K_S filter, to yield the final magnitudes.

Figure 1 shows examples of Spectral Energy Distributions (SEDs) for star cluster models at two different ages of 1 and 13 Gyr, and all five metallicities for each of them. The SEDs shown have been scaled to match the g-band magnitude of a solar metallicity star clusters with initial mass 10^6 $M_\odot$. Fluxes in all filter bands of course scale with cluster mass. At both ages the lines representing the different metallicities split up towards both longer and shorter wavelengths. We exploit this to separate the effects of age and metallicity.

2.1 AnalySED

To obtain accurate ages, metallicities and masses for the detected clusters we used the SED analysis tool AnalySED developed by Anders et al. (2004). This program compares the observed SED of a star cluster with a large grid of model SEDs and finds the best-fitting match to the observations. In this process ages and metallicities for each cluster are derived from the observed spectral energy distributions. Once

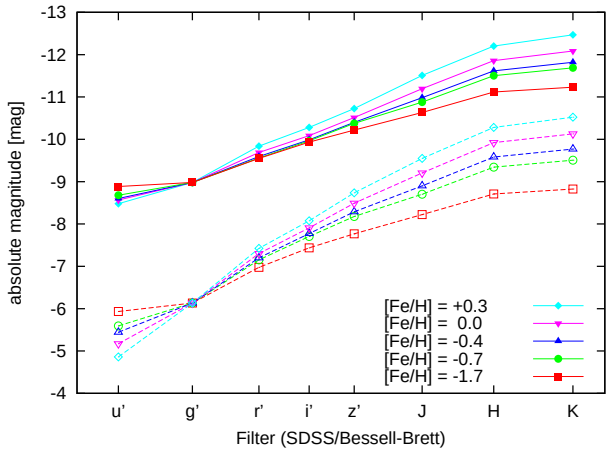

Figure 1. Spectral energy distributions (SEDs) for star cluster models at two different ages of 1 Gyr at brighter and 13 Gyr at fainter absolute magnitudes, respectively, and 5 different metallicities ranging from $1/50\,Z_\odot$ to $2.5\,Z_\odot$ in each case. All SEDs have been scaled to match the g-band magnitude of the solar metallicity model with initial mass 10^6 $M_\odot$.

those parameters are found the observed brightnesses are translated into masses.

Since we keep the full χ^2 distribution and not only the best fitting solution we are able to determine the 1σ uncertainties for all our derived parameters by summing up the normalized probabilities sorted from the highest to the lowest values until an integrated probability of 0.68 is reached. The uncertainty ranges for the different parameters are then given by their extreme values reached within this 1σ probability range (cf. Anders et al. (2004) for details of the method and e.g. Anders et al. (2004) for an earlier application).

3 OBSERVATIONS AND DATA REDUCTION

3.1 Near-infrared data

We observed NGC 4570 in two subsequent nights (2nd to 4th March 2007) using the ESO-NTT equipped with the SOFI near-infrared imager. This instrument consists of a Hawaii HgCdTe 1K×1K chip and $0.288''$ pixels yielding a field-of-view of $\approx 5 \times 5$ arcmin. To avoid non-linearities of the detector we chose an detector integration time (DIT) of 6 seconds. 12 of these exposures were internally averaged by the readout electronics, resulting in an exposure time per frame of 72 seconds. Since NGC 4570 has an extent of only $4' \times 1.1'$, we could use one half of the chip for the object while obtaining a simultaneous sky-exposure in the other half of the chip, swapping sides after each exposure and applying small shifts to avoid contamination by bad pixels.

3.1.1 Reduction

Data reduction largely followed the procedures outlined in the SOFI instrument handbook. The individual frames were corrected for the inter-row cross-talk and then corrected with a flat-field to remove pixel-to-pixel sensitivity variations. These flat-fields consisted of three different components: dome-flats corrected for their characteristic on-off pattern using the recipe provided on the NTT-SOFI website; illumination correction surface obtained from repeated observations of a standard star at different positions of the detector to remove the illumination gradient introduced by the dome flats; a "super-flat" created from the sky frames of both nights to remove remaining inhomogeneities and cosmetics from dust on the filter. Since the observations were carried out under non-photometric conditions we used the data from the instruments web-page[1] to obtain the illumination correction.

After flat-fielding all the frames we estimated the background in all frames by iteratively clipping values larger then 3σ above the mean of the full frame. We then used six sky-frames that were obtained closest in time, scaled each of them individually to the sky-value of the object frame and subtracted their average from the object frame. We varied the number of frames to average, but found that six is the best compromise between signal-to-noise and artifacts introduced by the pupil-rotation of the alt-az mounted telescope.

All the sky-subtracted frames were aligned by matching coordinates of several background galaxies in each frame to coordinates in a reference frame; we used galaxies instead of stars because due to the high galactic longitude there were too few stars to allow for proper matching. In a final step we stacked all but those frames with a sky-value deviating more than 2σ from the average.

Combining all those exposures from both nights results a total exposure time for our K-band image of $t_{exp} \approx 25$ ks $\approx$ 9.5 hours.

3.1.2 Photometric calibration

We could not base our photometric calibration on standard stars, because during both nights observations were hampered by a varying degree of cloudiness. We therefore compared brightness profiles of the host galaxies with calibrated data from the 2MASS survey (see Skrutskie et al. (2006) for a review) and own observations obtained later with the SIRIUS instrument at the InfraRed Survey Facility at the South African Astronomical Observatory. Both results showed excellent agreement within the error ranges of $\Delta m_K \approx 0.03$ mag, that can easily be explained by minor differences in the filter transmission curves. However, we account for this uncertainty by adding the calibration error in quadrature to the photometric errors. Calibration of exposures from both 2MASS and SIRIUS finally relied on standard stars from the Persson et al. (1998) catalog, so our K-band magnitudes are in the VEGA magnitude system.

This allows us to detect point sources down to $m_{Ks} \approx 21$ mag at the 10σ-level, making the depth of our observations comparable to deep surveys obtained with the same configuration, e.g. the K20 survey (Cimatti et al. 2002).

3.2 HST data

The HST data consisted of two datasets taken with the Advanced Camera for Survey (ACS) on-board the Hubble space telescope as part of the ACS Virgo cluster survey

[1] http://www.ls.eso.org/lasilla/sciops/ntt/sofi/

(Côté et al. 2004). For both datasets with filters F475W (≈ SDSS g) and F850LP (≈ SDSS z) we relied on the On-the-fly reduction performed automatically upon retrieval from the MAST Archive[2] and using the best reference files. We then performed an additional alignment step to ensure a match of coordinates in both frames as good as possible.

Calibration of the HST data was done using the appropriate header entries from the fits-files. For details on this process see the HST Data Handbook (Pavlovsky et al. 2005). To avoid any unnecessary conversion between different magnitude systems, we performed photometry in both HST filters using ST magnitudes.

3.3 Cluster selection

Globular Cluster candidates were selected from the HST images using SExtractor (Bertin & Arnouts 1996). A valid detection is characterized by at least 4 adjacent pixels with intensities of 3σ above the local background, resulting in two catalogs with > 1000 objects each. We then cross-correlated these catalogs to remove remaining spurious detections as e.g. remaining cosmics.

For the ≈ 330 remaining candidates we derived intrinsic source sizes using the ISHAPE-package from BAOLAB (Larsen 1999). This algorithm in our case convolves a King profile with a fixed concentration parameter $c = \frac{r_t}{r_c} = 30$ (or equivalently $\log(\frac{r_t}{r_c}) \approx 1.5$) but variable radii with the instrumental point spread function (PSF) created by TinyTim (Krist 2004) and determines the best fitting radius via χ^2-minimization. We rejected all objects appearing stellar-like (intrinsic radius $r_i < 0.2$ px ≈ 0.8 pc at a distance D ≈ 17 Mpc (Tonry et al. 2001), 17 objects) or too extended ($r_i > 5$ px ≈ 20 pc, 37 objects) to be a globular cluster.

3.4 Photometry

For the remaining ≈ 280 GC candidates we obtained aperture photometry using commands from the ESO-MIDAS package. For the HST images we used an aperture radius of 15 pixels and a sky annulus from 17 to 20 pixels. To compensate for the low-intensity extended wings of the ACS PSF we applied an aperture correction of 0.067 (0.082) mag to the F475W (F850LP) magnitudes according to the tabulated Enclosed Energy values of 0.940 (0.927) determined by Sirianni et al. (2005). Although these factors still depend both on the position of the GC on the detector and intrinsic colour of the GC, the implied uncertainties are much smaller then the photometric uncertainties and can therefore be neglected.

To derive photometry for the ground-based K_s-imaging we transformed the coordinates from the combined HST catalog into physical coordinates in the K-image and then used these coordinates as center positions for the photometry. Using SExtractor to also obtain a K-band detection catalog yielded less reliable results and missed many of the sources found with the superior resolution of the HST. We used an aperture of 2″ and an aperture correction derived from stellar photometry within the field-of-view of (0.2 ± 0.03) mag. For 117 candidates we could not derive a K-band magnitude, mostly because they were not included within or too near to the edge of the K-band field-of-view, and in some cases because they were out-shined by the bright galaxy background.

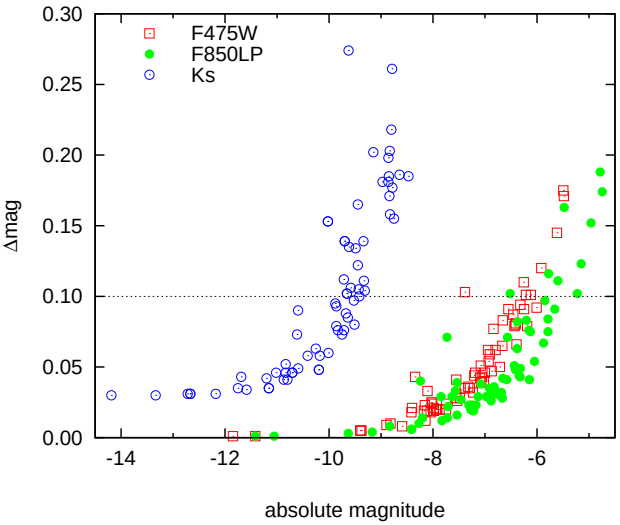

Figure 2. Photometric errors as function of absolute magnitudes for the HST filters F475W and F850LP and the NTT filter K_s.

To remove last outliers we introduced a colour selection criterion of $(g_{ST} - z_{ST}) \leqslant 1.0$ and $(z_{ST} - K_{s,Vega}) \leqslant 4.5$, covering the color range of our models. We further removed all candidates with magnitude errors $\geqslant 0.1$ mag in g and z and $\geqslant 0.3$ mag in K_s (see Fig. 2 for the distributions of magnitude uncertainties as a function of luminosity in all three bands). This leaves us a final sample of 63 *bona fide* GCs.

4 RESULTS

For three selected clusters we present the detailed χ^2 distributions in Fig. 3. This Fig. demonstrates that the reason for the uncertainties in the derived parameters are mostly relatively to isolated secondary peaks in the probability distribution. The cluster in the upper panel has a well-defined best-fit age of $1.12^{+0.90}_{-0.33}$ Gyr, a metallicity of [Fe/H] $= -0.3^{+0.3}_{-0.4}$ and a derived mass of $(2.64^{+1.59}_{-0.25}) \times 10^5$ $M_\odot$. Its χ^2 value for the best solution with [Fe/H] $= -0.4$ is a factor of 10 better than that for the somewhat lower metallicity [Fe/H] $= -0.7$ paired with slightly higher age. The cluster in the middle panel has an age of $16.0^{+0.00}_{-10.9}$ Gyr, a metallicity of [Fe/H] $= -1.7$ and a derived mass of $(4.81^{+0.00}_{-2.87}) \times 10^5$ $M_\odot$. It is clearly seen that the old age low metallicity solution has a χ^2-value about two orders of magnitude better than that for any other metallicity. Also the intermediate age solution for the same metallicity has a significantly higher χ^2. The cluster in the lower panel has an age of $5.62^{+10.4}_{-4.39}$ Gyr, a metallicity of [Fe/H] $= -1.7$ and a derived mass of $(9.96^{+13.6}_{-7.33}) \times 10^5$ $M_\odot$. Note the large age uncertainty for this cluster, that directly influences the derived mass of the cluster. Again, however, only the lowest metallicity gives an acceptable fit. Note that since our grid of models does not sample the covered metallicity range finely enough. Therefore only the lowest metallicity model results in a good fit

[2] http://archive.stsci.edu/

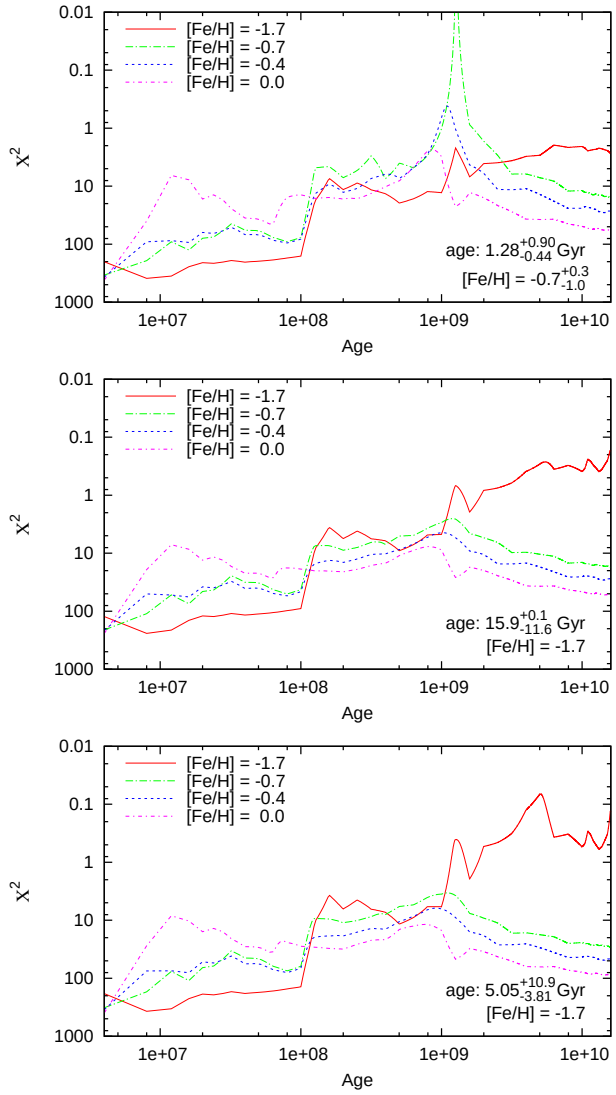

Figure 3. χ^2 values as function of metallicity and age for 3 different clusters.

hence we do not give errors on metallicity for those two clusters.

These three GCs represent typical cases for a very good fit with a fairly well constrained age, a securely old (> 5 Gyr) but less well constrained age, and a poorly constrained age, respectively.

4.1 Ages

Figure 4 shows the age distribution of all the GCs from our final sample. At old ages (age $> 10^{10}$ yr) we see the analogues to our old Milky Way GCs formed during an early phase of galaxy formation.

We also find a significant population of younger GCs with ages of $1 - 3$ Gyr that must have formed during some violent star formation event. Possible candidates for such events are massive bursts of star and star cluster formation that come along with a merger of two gas-rich spirals or the accretion of a gas-rich companion.

While the light grey histogram in Fig. 4 shows the

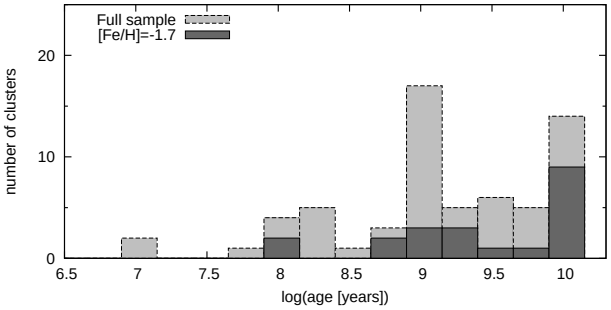

Figure 4. Age distribution of our detected globular clusters.

age distribution of all our GCs, the dark histogram shows metal-poor GCs only. The old peak contains GCs with [Fe/H]$= -1.7$ close to the metallicity of the halo GCs in our Milky Way, but also more metal-rich GCs while the intermediate-age peak is predominantly made up by GCs with metallicities higher than [Fe/H]$= -1.7$.

A detailed look at the 8 GCs in the log(age) bins 8.65-8.9 and 9.15-9.4 shows that within their error bars they might as well be part of the 8.9-9.15 Gyr peak. The GCs in the age bins 9.4-9.9, on the other hand, could, within their 1σ uncertainties as well be part of the truely old, i.e. $10 - 13$ Gyr population.

4.1.1 Old and metal-rich GCs

4 out of the 10 old clusters have SEDs best described by solar metallicity. This, however, does not seem very plausible, since it would require an incredibly fast global chemical enrichment to solar metallicity within a timescale of only about a Gyr. On nearer inspection, one of these four GCs has a large age uncertainty ranging down to 1.25 Gyrs, so it might well belong to our newly detected intermediate age population. The three remaining GCs are located within the extent of the host galaxy, so that their photometry might still be contaminated by light from the surrounding galaxy. This is also supported by the poor quality of their SED-fit with remarkably low unnormalized integrated probabilities $\lesssim 10^{-10}$.

4.2 Spatial distribution

There is no obvious difference in the spatial distributions of the old and younger GCs, as seen in Fig. 5. GC numbers, however, are too small for meaningful statistical tests.

We note that the bulk of the GCs we detect belong to the red peak of the optical GC colour distribution. Only the very brightest GCs from the blue optical peak are detected in K_s and, hence, part of our sample.

4.3 Metallicities

The metallicity distribution (Fig. 6) is dominated by a large population of 27 out of 63 clusters with solar metallicity, only 21 clusters have very low metallicities of [Fe/H] $= -1.7$ in the range of Galactic old GCs.

The fact that we find only relatively few old and metal-poor GCs can be explained as a selection effect: Since we

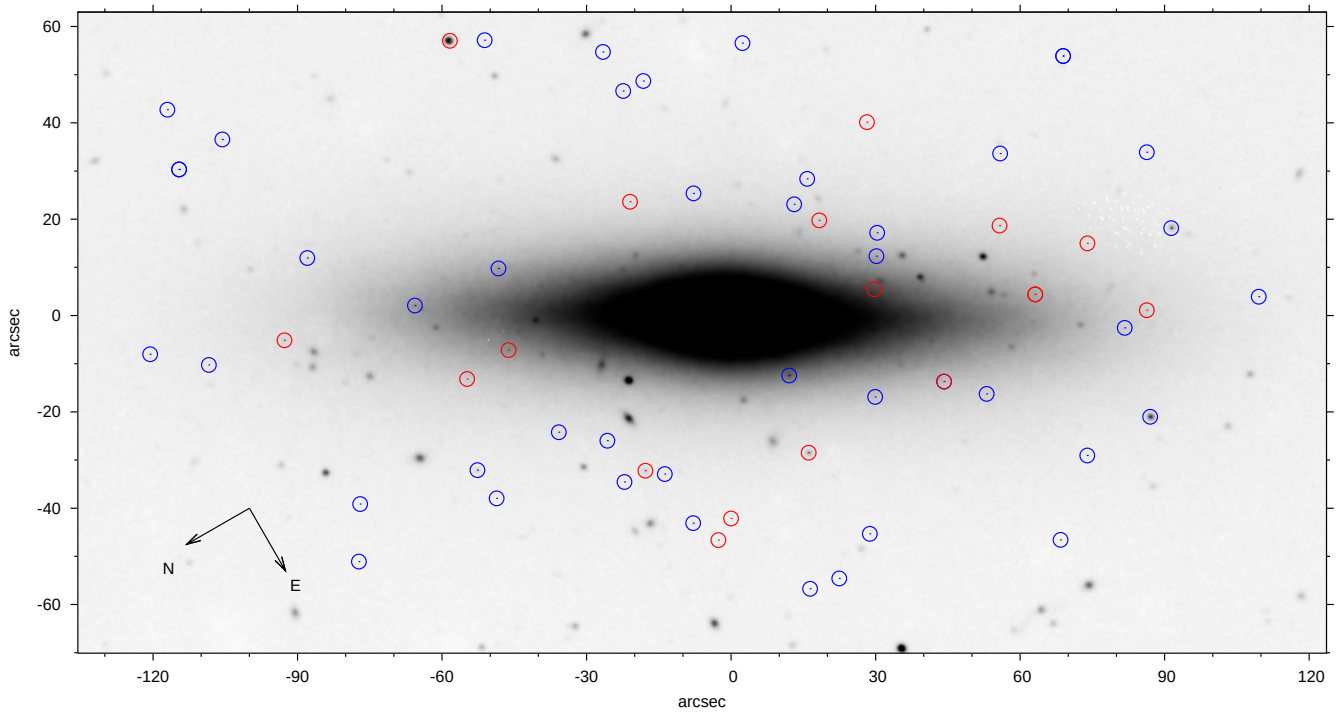

Figure 5. Spatial distribution of our Globular Cluster sample, overlayed over our K-band image obtained with NTT/SOFI. Blue circles mark GCs with best-fit ages < 3 Gyr, while red circles mark GCs older than 3 Gyr. Most of the bright sources are either stars or (in most cases) background galaxies, that are resolved on the HST images.

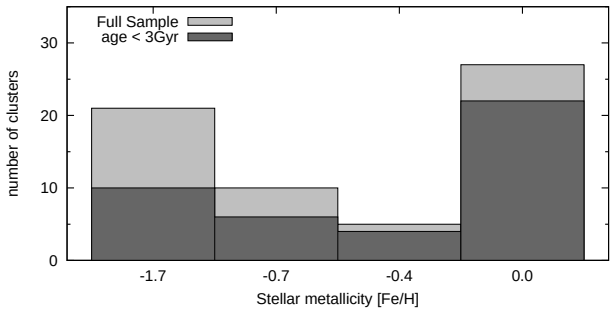

Figure 6. Metallicity distribution of our GCs. Light grey histogram: all GCs, dark: GC with ages younger than 5 Gyr.

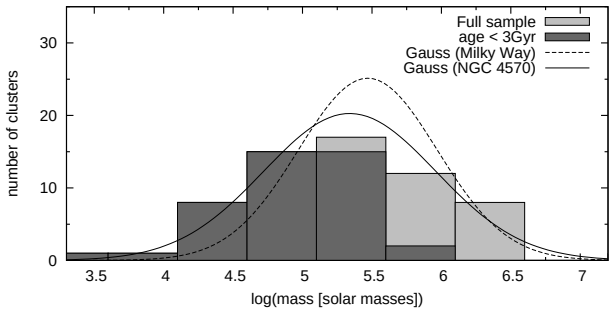

Figure 7. Mass distribution of the GCs in NGC 4570. The light grey histogram is for all GCs from our sample, the dark one for the subsample of GCs younger than 3 Gyr. The solid line is a Gaussian fit to our unbinned GC mass distribution with a median of $\log(\langle \mathrm{M_{GC}[M_\odot]} \rangle) = 5.3$ and $\sigma(\mathrm{M_{GC}}) = 0.6$ dex, normalized to the number of GCs in our sample. The dotted line gives the Gaussian for the Milky Way GCs with $\log(\langle \mathrm{M_{GC}[M_\odot]} \rangle_{\mathrm{MW}}) = 5.47$ and $\sigma_{\mathrm{MW}}(\mathrm{M_{GC}}) = 0.50$ dex, normalized to the number of GCs in our sample.

only include clusters that were also detected and also have good photometry in K_s we prefer intrinsically red objects. Old Milky Way-type globulars, however, have blue colors due to their low metallicity and are hence not included in our sample. Indeed, the bulk of all our GCs, and of the metal-rich ones in particular, are younger than 3 Gyr, again a selection effect, since 3 Gyr old GCs are brighter than 13 Gyr old ones by 1.1 to 1.3 mag, depending on metallicity and filter.

4.4 Masses

Fig. 7 shows the mass distribution of our GCs, again for the full sample in light grey and for the subsample of GCs with ages < 3 Gyr in dark grey. The mass distribution of the full GC sample clearly looks like a Gaussian with a turn-over mass around $\log(\langle \mathrm{M_{GC}[M_\odot]} \rangle) = 5.3$ and $\sigma(\mathrm{M_{GC}}) = 0.6$ dex, very similar to the turn-over of the GC mass function in the Milky Way which occurs at $\log(\langle \mathrm{M_{GC}[M_\odot]} \rangle_{\mathrm{MW}}) = 5.47$ with $\sigma_{\mathrm{MW}}(\mathrm{M_{GC}}) = 0.50$ dex (Ashman et al. 1995). The fact that the mass distribution of the young GCs does not extend to the same high masses as that for the old ones cannot be a selection effect, since more massive clusters of young age would be easily detectable if they were there. It seems that the sec-

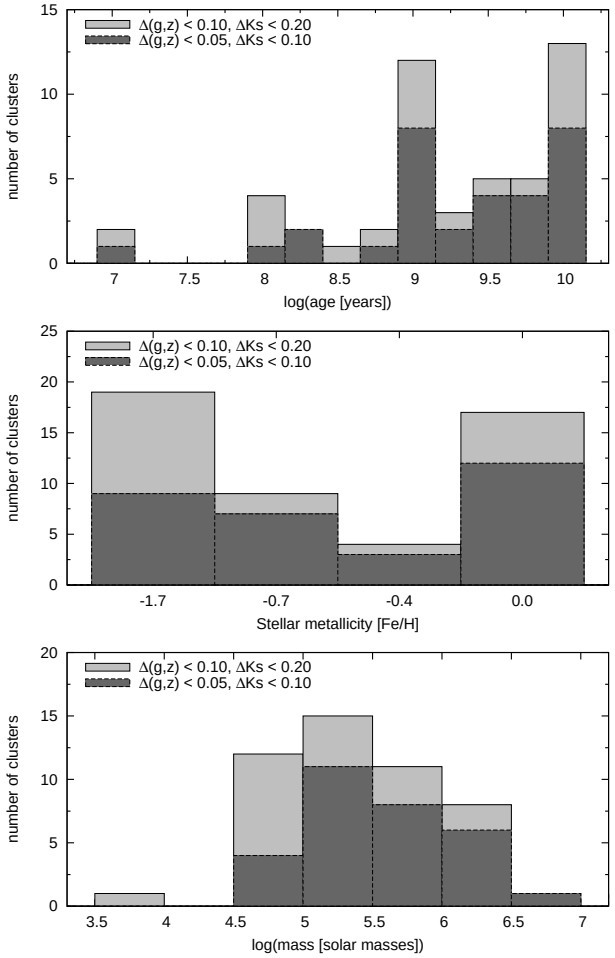

Figure 8. Age, metallicity, and mass distributions for the subsample of GCs with high (light grey) and very high (dark grey) photometric accuracies.

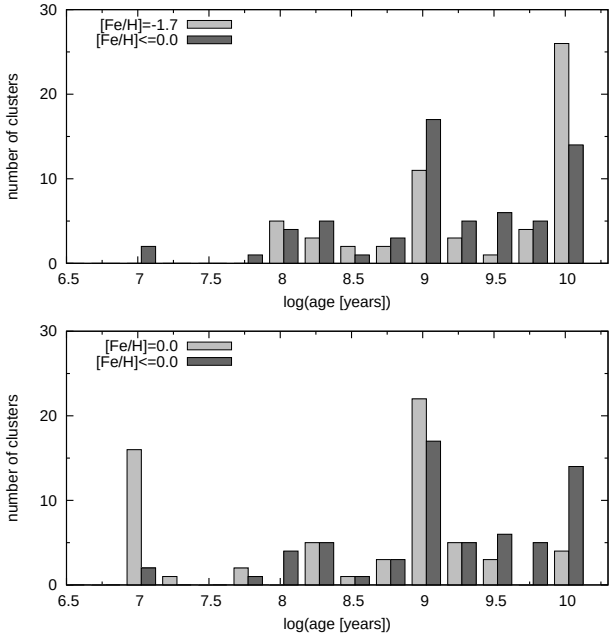

Figure 9. Age distributions of our GC sample under the assumption of a fixed low metallicity [Fe/H] = −1.7 (upper panel) and [Fe/H] = 0.0 (lower panel). Bin sizes are the same as in Fig 4, only the two histograms for free and restricted metallicities are plotted next to each other to better reveal the differences.

ondary event that formed the ∼ 2 Gyr old GCs in NGC 4570 did not form the GCs with the same mass function as the old GC population. Careful modeling of cluster destruction effects were required to really prove this conjecture. Dynamical friction, which is most important for massive clusters, might have preferentially destroyed those, in particular if the secondary GC population were more centrally concentrated than the primary one, as previously found in many, but not all, bimodal GC systems. In addition to that we might have missed massive GCs in front of the bright galaxy background if they either were initially closer to the centre (mass segregation) or driven towards the centre by dynamical friction faster than the lower mass ones.

4.5 The subsample of GCs with high photometric accuracy

In Fig. 8 we present our results for the age, metallicity, and mass distributions of the subset of GCs from our sample with the best photometric accuracies: $\Delta g, \Delta z < 0.10$, $\Delta K_s < 0.20$ mag and $\Delta g, \Delta z < 0.05$, $\Delta K_s < 0.10$ mag, respectively. This Fig. shows that our results are unaffected by the slightly higher uncertainties in our full sample. The age, metallicity, and mass distributions are robust. High photometric accuracies are only achieved for the brightest clusters. Hence it is no surprise that the high accuracy subsample lacks some of the low mass GCs.

4.6 Alternative solutions

4.6.1 Ages for fixed metallicities [Fe/H] = −1.7 *or* [Fe/H] = 0.0

In this subsection we explore to what extent our results change if we artificially restrict the allowed parameter range. Our aim is to see whether our basic finding of $\sim 1-3$ Gyr old/young GCs in NGC 4570 is affected by these assumptions.

If we limit the available parameter range to a metallicity [Fe/H] = −1.7 (see. upper panel of Fig 9 for comparison) many clusters are better described by older ages. These are needed to counter-balance the bluer colours of the lower metallicity models. The older ages, in turn, also result in slightly higher masses. However, the principle structure of the age distribution and, in particular, the peak at intermediate ages of 1–3 Gyr remain. This "worst-case" scenario emphasizes the robustness of our cluster age determination.

We also determined ages for a metallicity fixed to the solar value and again found little difference compared to the original results (see lower panel of Fig. 9). Although clusters on average get slightly younger in this case, the peak of the distribution around 1–3 Gyr still remains, only the tail towards younger ages become slightly more pronounced.

We conclude, that our finding of a substantial population of intermediate-age GCs with ages of order 1 – 3 Gyr

and approximately solar metallicities in NGC 4570 is very robust, even under extreme test changes in metallicity.

5 DISCUSSION

5.1 Formation scenarios for red-peak GCs

Our detection of a substantial population of 1 – 3 Gyr old GCs is most naturally explained in terms of a merger or accretion event which involved significant amounts of gas and triggered a strong starburst in which, together with some hitherto undetected population of field stars, the presently observed GC formed. The star clusters we find have all the properties of GCs, they are compact with half-light radii of order 3–7 pc and have masses in the range of typical GC masses. Those clusters that we observe with ages of 1 – 3 Gyr certainly are only a small fraction of all the star clusters formed in such an event. They have already survived the most dangerous phase in their lives, the infant mortality and dynamical restructuring phase after the first SNe have expelled the gas left-over from their formation. They probably have also survived the violent relaxation phase that restructured the merging/accreted galaxies into the presently observed S0. The sheer number of young GCs requires substantial gas masses involved and their high metallicities indicate that it could not have been a minor accretion event involving e.g. an SMC type galaxy swallowed by some major gas-free/poor E/S0/Sa type galaxy. Solar metallicities in the ISM out of which the new GCs were formed require at least one Sbc- or Sb-type progenitor. Sa-type galaxies have higher metallicities, but lack the required amounts of gas to fuel the starburst.

It is intriguing that the age we find for the young GCs agrees very well with the stellar population age of $\leqslant$ 2 Gyr estimated by van den Bosch & Emsellem (1998) for the nuclear stellar disk in the host galaxy (van den Bosch et al. 1998; van den Bosch & Emsellem 1998; Scorza & van den Bosch 1998). Our detection of a substantial population of GCs does not, however, support the internal bar instability scenario they favor for the formation of this nuclear stellar disk. Nuclear stellar disks are in fact seen in dynamical simulations of galaxy mergers/accretion events (cf. Bournaud et al. 2004; Springel & Hernquist 2005), as well as in real merger remnants, e.g. in Arp 214 and Arp 224 (Jog & Chitre 2002). The fact that NGC 4570 does not feature any obvious tidal tails can be understood as a consequence of its location in a high galaxy density region of the Virgo cluster, where tidal tails are shred down as soon as they start to develop.

We hence suggest that the young GCs we detected and the nuclear stellar disk in NGC 4570 have been formed by the same merger/accretion event.

6 FUTURE PROSPECTS

HST NIC3 data would be very valuable in order to detect young GC closer to the centre of NGC 4570 and see whether the young GC system is more centrally concentrated than the old one or not. Of equal value would be an extension of the SED to shorter wavelengths. As can also be seen from Figure 1 for both old and young clusters the U-band is both sensitive to ages and metallicity and can help discriminate between both. However, imaging in further intermediate band-passes would only be necessary for other galaxies containing dust (for further details see Anders et al. 2004). Spectroscopy, albeit challenging, would allow to confirm and eventually further constrain the photometric ages, metallicities and masses for these young GCs, while abundance ratios, e.g. of [α/Fe] could give further clues to the progenitor galaxies and to the star cluster formation scenario.

A natural next step seem to combine our results from this GC analysis with a detailed analysis of the stellar population across the main body of the galaxy to evaluate the contribution (and location) of field stars from the age range of the young GCs. This could either be done on the basis of multi-band imaging in a pixel-by-pixel analysis of the kind we did for the Tadpole and Mice galaxies (de Grijs et al. 2003) or analyzing the integrated spectrum with starburst models as we have done for the $\sim$ 1 Gyr old merger remnant NGC 7252 (cf. Fritze-v. Alvensleben & Gerhard 1994a,b).

7 SUMMARY

On the basis of deep NTT-SOFI K_s- band imaging in conjunction with archival HST ACS deep optical imaging we identified a substantial population of star clusters with ages in the range 1 – 3 Gyr and metallicities around solar in the Virgo S0 galaxy NGC 4570. All these clusters are compact with half-light radii in the range 3–7 pc and have masses of order 10^5 $M_\odot$. They have successfully survived their infant mortality phase and, hence, merit to be called young GCs. The clusters we detect in K_s make up an important fraction of the red peak of the bimodal GC optical colour distribution reported by Peng et al. (2006) from the ACS Virgo Cluster Survey.

We performed a number of test that showed our results to be robust.

The ages we find for the young GCs agree well with stellar population ages previously determined for the nuclear stellar disk in NGC 4570. We suggest that both the nuclear stellar disk and the young GC population have been formed in the same merger/accretion event. The presently observed GCs certainly are only a small part of the originally formed star cluster population, since only a small fraction of clusters usually survives until ages of $\geqslant$ 1 Gyr. The sheer number of young GCs suggests that the merger/accretion event must have involved substantial gas masses, the high metallicity of the new GCs suggests that the gas involved in this event must have been enriched at least to a level observed in present-day Sbc galaxies.

Our analysis has shown that GC populations are valuable tracers of their parent galaxy's star formation, chemical enrichment, and mass assembly histories.

Clearly further analyses, in particular of the stellar population across the main body of NGC 4570, are required before we fully understand the details of the scenario that gave rise to the present-day Virgo S0 NGC 4570 with its nuclear stellar disk and young GCs.

ACKNOWLEDGMENTS

We thank the International Space Science Institute (ISSI) for their hospitality and research support and our anonymous referee for very insightful comments that helped improve and clarify this paper. We are also grateful to Hagen Meyer who obtained the calibration data at the IRSF. RK thanks the ESO-NTT crew, Valentin Ivanov, Alessandro Ederoclite, and Monica Castillo, for support during the preparation and execution of the observations.

This publication is based on observations made with ESO Telescopes at the La Silla Observatory under programme ID 079.B-0511. This paper is also based on archival observations with the NASA/ESA Hubble Space Telescope, obtained at the Space Telescope Science Institute, which is operated by the Association of Universities for Research in Astronomy (AURA), Inc, under NASA contract NAS 5-26555.

REFERENCES

Anders P., Bissantz N., Fritze-v. Alvensleben U., de Grijs R., 2004, MNRAS, 347, 196
Anders P., de Grijs R., Fritze-v. Alvensleben U., Bissantz N., 2004, MNRAS, 347, 17
Anders P., Fritze-v. Alvensleben U., 2003, A&A, 401, 1063
Ashman K. M., Conti A., Zepf S. E., 1995, AJ, 110, 1164
Ashman K. M., Zepf S. E., 1992, ApJ, 384, 50
Beasley M. A., Baugh C. M., Forbes D. A., Sharples R. M., Frenk C. S., 2002, MNRAS, 333, 383
Bertin E., Arnouts S., 1996, A&AS, 117, 393
Bournaud F., Combes F., Jog C. J., 2004, A&A, 418, L27
Brodie J. P., Strader J., 2006, ARA&A, 44, 193
Cimatti A., Mignoli M., Daddi E., Pozzetti L., Fontana A., Saracco P., Poli F., Renzini A., Zamorani G., Broadhurst T., Cristiani S., D'Odorico S., Giallongo E., Gilmozzi R., Menci N., 2002, A&A, 392, 395
Côté P., Blakeslee J. P., Ferrarese L., Jordán A., Mei S., Merritt D., Milosavljević M., Peng E. W., Tonry J. L., West M. J., 2004, ApJS, 153, 223
Côté P., Piatek S., Ferrarese L., Jordán A., Merritt D., Peng E. W., Haşegan M., Blakeslee J. P., Mei S., West M. J., Milosavljević M., Tonry J. L., 2006, ApJS, 165, 57
de Grijs R., Lee J. T., Mora Herrera M. C., Fritze-v. Alvensleben U., Anders P., 2003, New Astronomy, 8, 155
Ferrarese L., Côté P., Jordán A., Peng E. W., Blakeslee J. P., Piatek S., Mei S., Merritt D., Milosavljević M., Tonry J. L., West M. J., 2006, ApJS, 164, 334
Forbes D. A., Brodie J. P., Grillmair C. J., 1997, AJ, 113, 1652
Fritze-v. Alvensleben U., 2004, A&A, 414, 515
Fritze-v. Alvensleben U., Gerhard O. E., 1994a, A&A, 285, 751
Fritze-v. Alvensleben U., Gerhard O. E., 1994b, A&A, 285, 775
Gebhardt K., Kissler-Patig M., 1999, AJ, 118, 1526
Hempel M., Hilker M., Kissler-Patig M., Puzia T. H., Minniti D., Goudfrooij P., 2003, A&A, 405, 487
Hempel M., Zepf S., Kundu A., Geisler D., Maccarone T. J., 2007, ApJ, 661, 768
Jog C. J., Chitre A., 2002, A&A, 393, L89
Kissler-Patig M., Brodie J. P., Minniti D., 2002, A&A, 391, 441
Krist J., 2004, TinyTim User's Manual. 6.3 edn
Kundu A., Whitmore B. C., 2001a, AJ, 121, 2950
Kundu A., Whitmore B. C., 2001b, AJ, 122, 1251
Larsen S. S., 1999, A&AS, 139, 393
Larsen S. S., Brodie J. P., Strader J., 2005, A&A, 443, 413
Mei S., Blakeslee J. P., Côté P., Tonry J. L., West M. J., Ferrarese L., Jordán A., Peng E. W., Anthony A., Merritt D., 2007, ApJ, 655, 144
Pavlovsky M., Biretta J., Bohlin R., Chiaberge M., Cox C., Dressel L., Fruchter A., Giavalisco M., Gilliland R., Gonzaga S., Koekemoer A., Lucas R., Mack J., Maiz-Apellaniz J., Mutchler M., , 2005, ACS Data Handbook, Version 4.0 (Baltimore: StScI)
Peng E. W., Jordán A., Côté P., Blakeslee J. P., Ferrarese L., Mei S., West M. J., Merritt D., Milosavljević M., Tonry J. L., 2006, ApJ, 639, 95
Persson S. E., Murphy D. C., Krzeminski W., Roth M., Rieke M. J., 1998, AJ, 116, 2475
Puzia T. H., Zepf S. E., Kissler-Patig M., Hilker M., Minniti D., Goudfrooij P., 2002, A&A, 391, 453
Salpeter E. E., 1955, ApJ, 121, 161
Schulz J., Fritze-v. Alvensleben U., Möller C. S., Fricke K. J., 2002, A&A, 392, 1
Scorza C., van den Bosch F. C., 1998, MNRAS, 300, 469
Sirianni M., Jee M. J., Benítez N., Blakeslee J. P., Martel A. R., Meurer G., Clampin M., De Marchi G., Ford H. C., Gilliland R., Hartig G. F., Illingworth G. D., Mack J., McCann W. J., 2005, PASP, 117, 1049
Skrutskie M. F., Cutri R. M., Stiening R., Weinberg M. D., Schneider S., Carpenter J. M., Beichman C., Capps R., 2006, AJ, 131, 1163
Springel V., Hernquist L., 2005, ApJ, 622, L9
Tonry J. L., Dressler A., Blakeslee J. P., Ajhar E. A., Fletcher A. B., Luppino G. A., Metzger M. R., Moore C. B., 2001, ApJ, 546, 681
van den Bosch F. C., Emsellem E., 1998, MNRAS, 298, 267
van den Bosch F. C., Jaffe W., van der Marel R. P., 1998, MNRAS, 293, 343
West M. J., Côté P., Marzke R. O., Jordán A., 2004, Nature, 427, 31